Journal of Reinforced Plastics and Composites 2008; 27; 167-186
originally published online Oct 31, 2007
DOI: 10.1177/0731684407081385

Static and free vibration analyses of laminated shells using a higher-order theory

S. Pradyumna[*] and J.N. Bandyopadhyay

Department of Civil Engineering, Indian Institute of Technology, Kharagpur 721302, India

ABSTRACT: A C^0 finite element formulation using a higher-order shear deformation theory is developed and used to analyze static and dynamic behavior of laminated shells. The element consists of nine degrees-of-freedom per node with higher-order terms in the Taylor's series expansion which represents the higher-order transverse cross sectional deformation modes. The formulation includes Sanders' approximation for doubly curved shells considering the effects of rotary inertia and transverse shear. A realistic parabolic distribution of transverse shear strains through the shell thickness is assumed and the use of shear correction factor is avoided. The shell forms include hyperbolic paraboloid, hypar and conoid shells. The accuracy of the formulation is validated by carrying out convergence study and comparing the results with those available in the existing literature.

KEYWORDS: Hyperbolic paraboliods; hypar; conoids; higher-order theory; finite element method.

INTRODUCTION

Shell structures are widely used in all industrial applications; especially those related to automobile, marine, nuclear, civil, aerospace and petrochemical engineering. In civil engineering construction, conoid, hyperbolic paraboloid and elliptic paraboloid shells are commonly used as roofing units to cover large column-free areas. Conoid shells (Figure 1-

[*] Corresponding Author, Tel.: +91-3222-283415; Fax: +91-3222-282254
E-mail address: pradyumna@civil.iitkgp.ernet.in (S. Pradyumna)
jnb@civil.iitkgp.ernet.in (J.N. Bandyopadhyay)

CON) provide ease of fabrication and allow sun light to come in. They are most suitable when greater rise is needed at one end. The hyperbolic paraboloid shells are aesthetically appealing and are used widely.

Laminated composites are important structural materials because of their high strength to weight and strength to stiffness ratios. The mechanical properties of the laminated composites depend on the degree of orthotropy of the layers, ratio of the transverse shear modulus to the in-plane shear modulus and stacking sequence of the laminate. By appropriate orientation of the fibres in each lamina, desired strength and stiffness can be achieved.

Study of static and dynamic behavior of laminated composite shells has gained much interest of many researchers from past few decades. In analyzing and designing complex structures, such as doubly curved shells, whose exact behavior pattern is difficult to conceive, it is deemed to fit to have a preliminary idea regarding the nature and magnitudes of displacements and stresses over the entire structure by adopting a simpler and cheaper method. Obtaining closed form solutions for such problems are complex; therefore, to efficiently and conveniently solve the problem, the finite element method is widely used. Many of the classical theories developed for thin elastic shells are based on the Love-Kirchhoff assumptions in which the normal to the mid-plane before deformation is considered to be normal and straight after the deformation. It underpredicts deflections and overpredicts natural frequencies and buckling loads. These deficiencies are mostly due to the neglect of transverse shear strains. The errors are even higher for structures made of advanced composites, whose elastic modulus to shear modulus ratios are very large. The first order shear deformation theory (FSDT) developed by Reissner [1] and Mindlin [2] considers a constant value of transverse shear strains through the thickness of the plate and thus requires shear correction factors. The shear correction factors are introduced to

account for the discrepancies between the constant state of shear strains in the FSDT and the parabolic distribution of shear strains in the elastic theory. Many researchers [3-10] developed higher-order theories in which the displacements of the middle surface are expanded as cubic functions of the thickness co-ordinate and the transverse displacement is assumed to be constant through the thickness. This displacement field leads to the parabolic distribution of the transverse shear stresses and, therefore, the use of shear correction factors is avoided.

Yang [3] developed a higher-order shell element with three constant radii of curvature, two principal radii, orthogonal to each other and one twist radius. The displacement functions *u*, *v* and *w* are composed of products of one-dimensional Hermite interpolation formulae. Reddy and Liu [4] modified Sanders' theory to develop a higher-order shear deformation theory of laminated elastic shells, which accounts for tangential stress free boundary conditions. They also presented Navier-type solutions for bending and free vibration problems. Shu and Sun [5] developed an improved higher-order theory for laminated composite plates. This theory satisfies the stress continuity across each layer interface and also includes the influence of different materials and ply-up patterns on the displacement field. Liew and Lim [6] proposed a higher-order theory by considering the Lamé parameter $(1+z/R_x)$ and $(1+z/R_y)$ for the transverse strains, which were neglected by Reddy and Liu [4]. This theory accounts for cubic distribution (non-even terms) of the transverse shear strains through the shell thickness in contrast with the parabolic shear distribution (even-terms) of Reddy and Liu [4]. Kant and Khare [7] presented a higher-order facet quadrilateral composite shell element. Bhimaraddi [8], Mallikarjuna and Kant [9], Cho et al. [10] are among the others to develop higher-order shear deformable shell theory. It is observed that except the theory of Yang [3], remaining

higher-order theories do not account for twist curvature ($1/R_{xy}$), which is very much essential while analyzing shell forms like hypar and conoid shells.

Static and dynamic analyses of shell panels were carried out by many researchers in the past few decades. Choi [11], with modified isoparametric element, analyzed the conoidal shells by adding four extra nonconforming displacement modes to transverse displacement. Ghosh and Bandyopadhyay [12, 13] studied bending behavior of conoidal shells using the finite element method and Galerkin method. Simplified bending analysis of doubly curved shells was done by Aditya and Bandyopadhyay [14] with modified boundary conditions. Chakravorty et al. [15,16] carried out finite element dynamic analysis of doubly curved shells which include hyperbolic paraboloids (Figure 2-HPR), hypars (Figure 3-HYP) and conoids. Stavridis [17], by analytical treatment of Marguerre equations with inertia terms added, studied free vibration of elliptical, hyperbolic paraboloid, hypar, conoid and soap bubble isotropic shells. The effects of presence of the stiffeners and the cutouts on these types of shells were studied by Nayak and Bandyopadhyay [18, 19]. Higher-order theories were widely used for free vibration analysis of laminated composite shells by many researchers [4, 6, 8, 20,21].

To the best of the authors' knowledge, however, literature is not available related to the application of higher-order theory for studying the static and dynamic behavior of laminated composite shells with the combination of all three radii of curvature. Therefore, in the present analysis, static and free vibration behavior of laminated composite anticlastic shells are studied. A Higher-order shear deformation theory (HSDT), developed by Kant and Khare [7], is used by extending it to the shells with all three radii of curvature.

THEORY AND FORMULATION

Let us consider a laminated shell element made of a finite number of uniformly thick orthotropic layers (Figures 4 and 5), oriented arbitrarily with respect to the shell co-ordinates (*x,y,z*). The co-ordinate system (*x,y,z*) is chosen such that the plane *x*-*y* at *z*=0 coincides with the mid-plane. In order to approximate the three-dimensional elasticity problem to a two-dimensional one, the displacement components *u(x,y,z), v(x,y,z)* and *w(x,y,z)* at any point in the shell space are expanded in Taylor's series in terms of the thickness co-ordinates. The elasticity solution indicates that the transverse shear stresses vary parabolically through the element thickness. This requires the use of a displacement field in which the in-plane displacements are expanded as cubic functions of the thickness co-ordinate. The displacement fields, which satisfy the above criteria are assumed in the form as given by Kant and Khare [7]

$$\begin{aligned} u(x,y,z) &= u_0(x,y) + z\theta_y + z^2 u_0^*(x,y) + z^3\theta_y^*(x,y) \\ v(x,y,z) &= v_0(x,y) - z\theta_x + z^2 v_0^*(x,y) - z^3\theta_x^*(x,y) \\ w(x,y,z) &= w_0 \end{aligned} \tag{1}$$

where *u, v* and *w* are the displacements of a general point (*x,y,z*) in an element of the laminate along *x, y* and *z* directions, respectively. The parameters u_0, v_0, w_0, θ_x and θ_y are the displacements and rotations of the middle plane, while u_0^*, v_0^*, θ_x^* and θ_y^* are the higher-order displacement parameters defined at the mid-plane.

The linear strain-displacement relations according to Sanders' approximation are,

$$\varepsilon_x = \frac{\partial u}{\partial x} + \frac{w}{R_x},\ \varepsilon_y = \frac{\partial v}{\partial y} + \frac{w}{R_y},\ \gamma_{xy} = \frac{\partial v}{\partial x} + \frac{\partial u}{\partial y} + \frac{2w}{R_{xy}},$$

$$\gamma_{xz} = \frac{\partial u}{\partial z} + \frac{\partial w}{\partial x} - C_1\frac{u}{R_x} - C_1\frac{v}{R_{xy}},\ \gamma_{yz} = \frac{\partial v}{\partial z} + \frac{\partial w}{\partial y} - C_1\frac{v}{R_y} - C_1\frac{u}{R_{xy}} \tag{2}$$

Substituting Equation 1 in Equation 2,

$$\varepsilon_x = \varepsilon_{x0} + z\kappa_x + z^2\varepsilon^*_{x0} + z^3\kappa^*_x$$
$$\varepsilon_y = \varepsilon_{y0} + z\kappa_y + z^2\varepsilon^*_{y0} + z^3\kappa^*_y$$
$$\gamma_{xy} = \gamma_{xy0} + z\kappa_{xy} + z^2\gamma^*_{xy0} + z^3\kappa^*_{xy}$$

$$\gamma_{xz} = \varphi_x + z\kappa_{xz} + z^2\varphi^*_x + z^3\kappa^*_{xz}$$
$$\gamma_{yz} = \varphi_y + z\kappa_{yz} + z^2\varphi^*_y + z^3\kappa^*_{yz} \tag{3}$$

where,

$$\left\{\varepsilon_{x0}, \varepsilon_{y0}, \gamma_{xy0}, \varepsilon^*_{x0}, \varepsilon^*_{y0}, \gamma^*_{xy0}\right\} = \left\{\frac{\partial u_0}{\partial x} + \frac{w_0}{R_x}, \frac{\partial v_0}{\partial y} + \frac{w_0}{R_y}, \frac{\partial u_0}{\partial y} + \frac{\partial v_0}{\partial x} + \frac{2w_0}{R_{xy}}, \frac{\partial u^*_0}{\partial x}, \frac{\partial v^*_0}{\partial y}, \frac{\partial v^*_0}{\partial x} + \frac{\partial u^*_0}{\partial y}\right\}$$

$$\left\{\kappa_x, \kappa_y, \kappa_{xy}, \kappa^*_x, \kappa^*_y, \kappa^*_{xy}\right\} = \left\{\frac{\partial \theta_y}{\partial x}, -\frac{\partial \theta_x}{\partial y}, \frac{\partial \theta_y}{\partial y} - \frac{\partial \theta_x}{\partial x} + C_0\frac{\partial u_0}{\partial y} - C_0\frac{\partial v_0}{\partial x}, \frac{\partial \theta^*_y}{\partial x}, -\frac{\partial \theta^*_x}{\partial y}, \frac{\partial \theta^*_y}{\partial y} - \frac{\partial \theta^*_x}{\partial x}\right\}$$

$$\left\{\varphi_x, \varphi_y\right\} = \left\{\frac{\partial w_0}{\partial x} + \theta_y - C_1\frac{u_0}{R_x} - C_1\frac{v_0}{R_{xy}}, \frac{\partial w}{\partial y} - \theta_x - C_1\frac{v_0}{R_y} - C_1\frac{u_0}{R_{xy}}\right\}$$

$$\left\{\varphi^*_x, \varphi^*_y\right\} = \left\{3\theta^*_y - C_1\frac{u^*_0}{R_x} - C_1\frac{v^*_0}{R_{xy}}, -3\theta^*_x - C_1\frac{v^*_0}{R_y} - C_1\frac{u^*_0}{R_{xy}}\right\} \tag{4}$$

$$\left\{\kappa_{xz}, \kappa_{yz}, \kappa^*_{xz}, \kappa^*_{yz}\right\} = \left\{2u^*_o - C_1\frac{\theta_y}{R_x} + C_1\frac{\theta_x}{R_{xy}}, 2v^*_o + C_1\frac{\theta_x}{R_y} - C_1\frac{\theta_y}{R_{xy}}, -C_1\frac{\theta^*_y}{R_x} + C_1\frac{\theta^*_x}{R_{xy}}, C_1\frac{\theta^*_x}{R_x} - C_1\frac{\theta^*_y}{R_{xy}}\right\}$$

C_1 is a tracer by which the analysis can be reduced to that of shear deformable Love's first approximation and $C_0 = 0.5\left(1/R_x - 1/R_y\right)$ is the result of Sander's theory which accounts for the condition of zero strain for rigid body motion.

The constitutive relations for a typical lamina *k* with reference to the fibre-matrix co-ordinate axis 1-2 (Figure 5) are written as,

$$\begin{Bmatrix}\sigma_1\\ \sigma_2\\ \tau_{12}\\ \tau_{13}\\ \tau_{23}\end{Bmatrix}^k = \begin{bmatrix}Q_{11} & Q_{12} & 0 & 0 & 0\\ Q_{12} & Q_{22} & 0 & 0 & 0\\ 0 & 0 & Q_{66} & 0 & 0\\ 0 & 0 & 0 & Q_{44} & 0\\ 0 & 0 & 0 & 0 & Q_{55}\end{bmatrix}^k \begin{Bmatrix}\varepsilon_1\\ \varepsilon_2\\ \gamma_{12}\\ \gamma_{13}\\ \gamma_{23}\end{Bmatrix}^k \tag{5}$$

or, in matrix form,

$$\{\sigma\}_k = [Q]_k \{\varepsilon\}_k$$

where, $Q_{11} = \frac{E_1}{1-\nu_{12}\nu_{21}}$, $Q_{12} = \frac{\nu_{12}E_2}{1-\nu_{12}\nu_{21}}$, $Q_{22} = \frac{E_2}{1-\nu_{12}\nu_{21}}$, $Q_{66} = G_{12}$, $Q_{44} = G_{13}$,

$Q_{55} = G_{23}$ and $\frac{\nu_{12}}{E_1} = \frac{\nu_{21}}{E_2}$

For the elastic constant matrix to any arbitrary axis with which the material principal axes make an angle θ, standard co-ordinate transformation is required. Thus, the off-axis elastic constant matrix is obtained from the on-axis elastic constant matrix using the relation

$\left[\overline{Q}_{ij}\right] = [T]^T \left[Q_{ij}\right][T]$, where [$T$] is the transformation matrix.

Therefore, the stress-strain relations for a lamina about any axis are given by,

$$\begin{Bmatrix} \sigma_x \\ \sigma_y \\ \tau_{xy} \\ \tau_{xz} \\ \tau_{yz} \end{Bmatrix}_k = \begin{bmatrix} \overline{Q}_{11} & \overline{Q}_{12} & \overline{Q}_{16} & 0 & 0 \\ \overline{Q}_{12} & \overline{Q}_{22} & \overline{Q}_{26} & 0 & 0 \\ \overline{Q}_{16} & \overline{Q}_{26} & \overline{Q}_{66} & 0 & 0 \\ 0 & 0 & 0 & \overline{Q}_{44} & \overline{Q}_{45} \\ 0 & 0 & 0 & \overline{Q}_{45} & \overline{Q}_{55} \end{bmatrix}_k \begin{Bmatrix} \varepsilon_x \\ \varepsilon_y \\ \gamma_{xy} \\ \gamma_{xz} \\ \gamma_{yz} \end{Bmatrix}_k \tag{6}$$

Integrating the stresses through the laminate thickness, the resultant forces and moments acting on the laminate are obtained.

$$\left[N, N^*\right] = \begin{bmatrix} N_x & N_x^* \\ N_y & N_y^* \\ N_{xy} & N_{xy}^* \end{bmatrix} = \sum_{k=1}^{N_L} \int_{z_k}^{z_{k+1}} \begin{bmatrix} \sigma_x \\ \sigma_y \\ \tau_{xy} \end{bmatrix} \left[1, z^2\right] dz$$

$$\left[M, M^*\right] = \begin{bmatrix} M_x & M_x^* \\ M_y & M_y^* \\ M_{xy} & M_{xy}^* \end{bmatrix} = \sum_{k=1}^{N_L} \int_{z_k}^{z_{k+1}} \begin{bmatrix} \sigma_x \\ \sigma_y \\ \tau_{xy} \end{bmatrix} \left[z, z^3\right] dz$$

$$[Q,S,Q^*,S^*]=\begin{bmatrix} Q_x & S_x & Q_x^* & S_x^* \\ Q_y & S_y & Q_y^* & S_y^* \end{bmatrix}=\sum_{k=1}^{N_L}\int_{z_k}^{z_{k+1}}\begin{bmatrix}\tau_{xz}\\ \tau_{yz}\end{bmatrix}\left[1,z,z^2,z^3\right] \tag{7}$$

or $\bar{\sigma}=D\bar{\varepsilon}$, where,

$$\bar{\sigma}=\left(N_x,N_y,N_{xy},N_x^*,N_y^*,N_{xy}^*,M_x,M_y,M_{xy},M_x^*,M_y^*,M_{xy}^*,Q_x,Q_y,Q_x^*,Q_y^*,S_x,S_y,S_x^*,S_y^*\right)^T$$

$$\bar{\varepsilon}=\left(\varepsilon_{x0},\varepsilon_{y0},\gamma_{xy0},\varepsilon_{x0}^*,\varepsilon_{y0}^*,\gamma_{xy0}^*,\kappa_x,\kappa_y,\kappa_{xy},\kappa_x^*,\kappa_y^*,\kappa_{xy}^*,\varphi_x,\varphi_y,\varphi_x^*,\varphi_y^*,\kappa_{xz},\kappa_{yz},\kappa_{xz}^*,\kappa_{yz}^*\right)^T$$

$[D]=\begin{bmatrix} D_m & D_c & 0 \\ D_c^T & D_b & 0 \\ 0 & 0 & D_s \end{bmatrix}$, where D_m, D_b, D_c and D_s are given in Appendix A

FINITE ELEMENT FORMULATION

An eight-noded isoparametric C^o element with nine degrees of freedom per node is used. The displacement vector d at any point on the mid-surface is given by:

$$d=\sum_{i=1}^{8}N_i(x,y)d_i$$

where d_i is the displacement vector corresponding to node i and N_i is the interpolating function associated with the node i.

Knowing the generalized displacement vector $\{d\}$ at all points within the element, the generalized mid-surface strains at any point given by Equation 3, are expressed in terms of global displacements in the matrix form as:

$$\bar{\varepsilon}=\sum_{i=1}^{8}B_i d_i \tag{8}$$

where B_i is a differential operator matrix of interpolation functions and obtained from Equation 4. The element stiffness matrix for the element e, which includes membrane, flexure and the transverse shear effects, and the element mass matrix are given by the following equations:

$$[K_e] = \int_{-1}^{1}\int_{-1}^{1} [B]^T [D][B]|J|\,drds$$

$$[M_e] = \int_{-1}^{1}\int_{-1}^{1} [N]^T [m][N]|J|\,drds$$

where [*N*] is the shape function matrix and [*m*] is the inertia matrix, as given in Appendix B. In all the numerical computations, the selective integration rule is employed. A 3×3 Gaussian rule is used to compute in-plane, coupling between in-plane and bending deformations, while a 2×2 rule is used to evaluate the terms associated with transverse shear deformation. The element mass matrix is evaluated using a 3×3 Gaussian rule. The element matrices are then assembled to obtain the global [*K*] and [*M*] matrices. The free vibration analysis involves determination of natural frequencies from the condition

$$([K] - \omega_n^2[M]) = 0$$

This is a generalised eigenvalue problem and is solved by using the subspace iteration algorithm.

RESULTS AND DISCUSSIONS

A computer program is developed based on the above formulation. A parallel program is developed based on the first order shear deformation theory (FSDT) in order to compare the results with those of HSDT. The shell-forms mainly considered here are hyperbolic paraboloid, hypar and conoid shells.

The following two boundary conditions are used in the present analysis:

(i) Simply supported boundary (S-S-S-S) having SS1 for isotropic and cross-ply laminates and SS2 for angle-ply laminates;

SS1: $v_0 = w_0 = \theta_y = v_0^* = \theta_y^* = 0,$ at $x = 0, a;$ $u_0 = w_0 = \theta_x = u_0^* = \theta_x^* = 0,$ at $y = 0, b.$

SS2: $u_0 = w_0 = \theta_y = u_0^* = \theta_y^* = 0,$ at $x = 0, a;$ and $v_0 = w_0 = \theta_x = v_0^* = \theta_x^* = 0,$ at $y = 0, b.$

(ii) Clamped boundary (C-C-C-C): $u_0 = v_0 = w_0 = \theta_x = \theta_y = u_0^* = v_0^* = \theta_x^* = \theta_y^* = 0,$ at x = 0, a and y = 0, b.

Non-dimensional length parameters are designated by $\bar{x} = x/a$ and $\bar{y} = y/b$.

Non-dimensional center deflection parameter $\bar{w} = (wh^3 E_2 / w_z a^4) \times 1000$.

Non-dimensional frequency parameter $\bar{\omega} = \omega a^2 / h\sqrt{(\rho / E_2)}$

Unless otherwise specified the elastic properties of the structure is taken as $E_1 / E_2 = 25$, $G_{12} = G_{13} = 0.5E_2$, $G_{23} = 0.2E_2$ and $\nu_{12} = 0.25$.

Validation of the present formulation

In order to validate the present formulation, the following problems are taken up from the existing literature.

Convergence study

First, convergence study is carried out in order to determine the uniform mesh size $N \times N$ at which the displacement values converge. Figure 6 shows the convergence results of a single layer SS1 spherical shell subjected to sinusoidal loading with $a/b = 1, a/h = 100, R_x = R_y = R$ and $R/a = 1$ with the orthotropic elastic properties as mentioned earlier. The obtained results are compared with the 3D results of Bhimaraddi [22]. The mesh size parameter N is varied from 2 to 10 and from Figure 6, it is found that the values of displacement converge for the N value 6. The subsequent analysis is carried out using the uniform mesh size of 6×6.

Comparison of results

1. A simply supported (SS1) three-layered symmetric cross-ply ($0^0/90^0/0^0$) rectangular plate of aspect ratio b/a=3 and subjected to sinusoidal load is considered here. Non-dimensional center deflection parameter for this problem is given by $\bar{w} = (wh^3 E_2 / w_z a^4) \times 100$. The obtained results are compared with those of Pagano [23]

employing three-dimensional elasticity theory and of Reddy [24] using higher-order plate theory and are listed in Table 1. It is found that the present HSDT results are in good agreement with the three-dimensional elasticity results given by Pagano [23] for all ratios of *a/h* considered here. However, it is also seen that FSDT gives fairly good results for thin plates, though fails to give satisfactory results for thick plates.

2. A spherical shell with $a/b=1$ and $R_x = R_y = R$ with SS1 boundary condition and subjected to sinusoidal loading is considered for the analysis. This problem was earlier solved by Bhimaraddi [22]. The lamination schemes considered here are single layered orthotropic and two layered cross-ply $0^0/90^0$. The purpose of taking this problem is to confirm that the present formulation gives consistent results even for single layered shells. The center displacements obtained are non-dimensionalised as wE_{22}/q, where q is the intensity of the sinusoidal load. Table 2 shows the non-dimensional center displacements of the spherical shell with thickness to side ratios (*h/a*) of 0.01, 0.1 and 0.15 and *R/a* ratios 1 to ∞ (plate) using both FSDT and HSDT formulations. From Table 2, it is found that the results obtained from the present HSDT formulation match well with the 3D results reported by Bhimaraddi [22].

3. A conoid shell with a = 2.521m, b = 1.828m, H_h = 0.457m, h_l = 0.228m, h = 12.7mm, E=38.843kN/mm^2, $\nu = 0.15$, with simply supported (SS1) boundary condition and subjected to a uniformly distributed pressure of 2.8734 x 10^{-3} N/mm^2 is considered for analysis. This problem was earlier solved by Choi [11]. Figure 7 shows the variation of transverse displacement (w) along $\bar{x}=0.5$ and $\bar{y}=0.5$ to 1.0. Figure 8 shows the variation of transverse displacement (w) along $\bar{x}=0$ to 1.0 and $\bar{y}=0$. In general, the results obtained from the present formulations are seen to be comparable with those of Choi [11].

4. Free vibration analysis is carried out for different types of shell geometry to compare the obtained frequency parameters with the available results. Frequency parameters $\bar{\omega}$ are

listed in Table 3 and found matching well with the available results of Nayak and Bandyopadhyay [19]. It is also observed that the frequency results from HSDT are on the lower side compared to FSDT results.

After validating the present HSDT results with those of available literature, the present HSDT is employed to study the static and dynamic behavior of shells with different geometries, loadings, boundary conditions and lamination schemes which are given in the subsequent sections.

Static analysis

To the best of authors' knowledge, no published results are available on the application of higher-order theories for static and dynamic analysis of shell forms like hypars and conoids. In the present work, HSDT is employed to carry out static and free vibration analyses on such shell forms.

Cross-ply laminated hypar shells having eight lamination schemes of $0^0/90^0$, $90^0/0^0$, $0^0/90^0/0^0$, $90^0/0^0/90^0$, $0^0/90^0/90^0/0^0$, $90^0/0^0/0^0/90^0$, $0^0/90^0/0^0/90^0$, and $90^0/0^0/90^0/0^0$ with simply supported and clamped boundary conditions and varying *c/a* ratios from 0 to 0.2 are subjected to uniformly distributed and sinusoidal loadings. Out of eight lamination schemes, four are antisymmetric ($0^0/90^0$, $90^0/0^0$, $0^0/90^0/0^0/90^0$ and $90^0/0^0/90^0/0^0$) having two and four layers respectively. The other four lamination schemes ($0^0/90^0/0^0$, $90^0/0^0/90^0$, $0^0/90^0/90^0/0^0$ and $90^0/0^0/0^0/90^0$) are symmetric having three and four layers. Common geometric parameters for all the hypar shells are $a/h = 100$ and $a/b = 1$. It may be noted that the *c/a* ratio is an indicator of the twist curvature of the hypar shell.

The non-dimensional central deflections of the two antisymmetric two layers lamination schemes ($0^0/90^0$ and $90^0/0^0$) are found to be the same for different *c/a* ratios subjected to both cases of loadings and boundary conditions. Similarly, the two

antisymmetric four layers lamination schemes $0^0/90^0/0^0/90^0$ and $90^0/0^0/90^0/0^0$ are also showing the same values of $\bar{w}$ for all the values of *c/a*, two different types of loadings and boundary conditions. It is interesting to note further that the two symmetric lamination schemes of both three layers ($0^0/90^0/0^0$ and $90^0/0^0/90^0$) and of four layers ($0^0/90^0/90^0/0^0$ and $90^0/0^0/0^0/90^0$) are also showing the respective identical values of $\bar{w}$ for different values of *c/a* for the two cases of loadings and boundary conditions.

Accordingly, Tables 4-7 present the values of $\bar{w}$ for four different lamination schemes having two, three and four layers for all the values of *c/a*, two types of loadings and boundary conditions. The least values of $\bar{w}$ are made bold in four tables for their easy identification.

The following discussion shows the influence of the boundary conditions, *c/a* ratio and lamination schemes on the non-dimensional central deflection $\bar{w}$ of the hypar shells subjected to two different types of loadings.

The reduction of the deflection with the increase of *c/a* ratio for all eight lamination schemes indicates the increase of the stiffness of the shell with the increase of twist curvature for the two types of boundary conditions and loadings.

The superiority of clamped boundary condition is observed (as expected) from the lower values of $\bar{w}$ when compared to those respective values with simply supported boundary condition for each of the two types of loadings. Needless to mention that this observation is for all values of *c/a*, lamination schemes and other constant values of different geometrical parameters and material properties as given in the notes below each of the Tables 4-7.

- The superior performance of $0^0/90^0/0^0$ lamination scheme having three symmetric layers when *c/a* = 0 (plate) is observed from the lowest value of $\bar{w}$

out of all the values furnished in Tables 4-7. Thus, it is inferred that the $0^0/90^0/0^0$ lamination scheme is best for plates for the two types of boundary conditions and loadings and geometrical parameters and material properties as mentioned in the earlier discussion.

- The superiority of the same $0^0/90^0/0^0$ lamination scheme is also observed for most of the cases of hypar shells (*c/a* from 0.05 to 0.2 in Tables 4, 5 and 7) for the two types of loadings and boundary conditions except for the simply supported hypar shells subjected to sinusoidal load (Table 6).
- In case of simply supported hypar shell subjected to sinusoidal load, the values of $\bar{w}$ from Table 6 reveals the superiority of lamination schemes of four layers (either symmetric $0^0/90^0/90^0/0^0$ for *c/a*=0.05 or antisymmetric $0^0/90^0/0^0/90^0$ for *c/a* ranging from 0.1 to 0.2).

Free vibration analysis

To study the free vibration behavior of different shell forms using HSDT, shells of three different geometries (hyperbolic paraboloid, hypar and conoid shell) are considered with three different boundary conditions: simply supported (S-S-S-S with SS2 conditions), clamped (C-C-C-C) and corner supported. The considered shell panels are antisymmetric angle-ply with three different lamination schemes (15^0/-15^0, 30^0/-30^0 and 45^0/-45^0). Table 8 gives the non-dimensional frequency parameter $\bar{\omega}$. A detailed study of the results of Table 8 shows the following two common observations regarding the increase of the stiffness of the shell as a result of having lower values of the non-dimensional frequency.

1. The C-C-C-C boundary condition shows the best performance with respect to the stiffness followed by S-S-S-S and corner supported boundary conditions for all three shell forms

2. The rigidity of shell becomes highest when h/R = -1/300 for hyperbolic paraboloids, c/a = 0.2 for hypars and h_l/H_h = 0.2 for conoids, as evident from the higher values of the respective $\bar{\omega}$, when compared to those with other values of h/R, c/a and h_l/H_h for hyperbolic paraboloids, hypars and conoids, respectively.

The above discussion of the results of Table 8 regarding the superiority of the shell regarding the stiffness is made considering the variation of the specific parameter and keeping the other parameters constant.

Figures 9 and 10 show the effects of h_l/H_h ratio on the frequency parameter ($\bar{\omega}$) for a S-S-S-S conoid shell of $a/h = 100$; $a/b = 1$ for four different lamination schemes with a/H_h ratios 2.5 and 5, respectively. Figures 11 and 12 also show the effect of h_l/H_h ratio on the frequency parameter ($\bar{\omega}$) for a clamped conoid shell. The superiority of the clamped conoid shell is evident from the higher values of $\bar{\omega}$ from Figures 11 and 12 as compared with those of Figures 9 and 10 for the S-S-S-S boundary condition. The range of variation of $\bar{\omega}$ is comparatively narrow for each of the four different orientations for the C-C-C-C conoids (Figures 11 and 12) than the same for the S-S-S-S conoids (Figures 9 and 10).

The values of $\bar{\omega}$ are increasing in Figures 9 and 10 with the increase of h_l/H_h for both the values of a/H_h as 2.5 and 5 when the boundary condition is S-S-S-S. This increase of $\bar{\omega}$ has two distinct zones in most of the stacking sequences; initially with steep and almost constant slope upto h_l/H_h around 0.3 and then with much reduced slopes. Critical study of Figures 9 and 10 further reveals marginal reduction of $\bar{\omega}$ in the second zone for some of the orientations when the boundary condition is simply supported for both the values of a/H_h as 2.5 and 5.

The nature of variation of $\bar{\omega}$ is somewhat different for the clamped conoids (Figures 11 and 12) for all four types of lamination scheme, where there is a tendency of reduction with the increase of h_l/H_h initially, followed by the increase of $\bar{\omega}$ at the later stage.

CONCLUSIONS

Static and free vibration analyses of laminated anticlastic shells are carried out using a higher-order theory taking into account all the three radii of curvature. From the present study the following conclusions are made:

1. A comparative study of the results of plates and different shell forms employing present formulation with those of available literature (Tables 1-3, Figures 7 and 8) shows that the present higher-order formulation gives fairly good results.

2. The three layer lamination scheme ($0^0/90^0/0^0$) is having the maximum stiffness showing the least deflection for plates (when c/a=0) subjected to two types of loadings and boundary conditions and with other constant values of geometric parameters and material properties (Tables 4-7).

3. The above three layer lamination scheme ($0^0/90^0/0^0$) also proves to have the maximum stiffness for most of the cases of hypar shells taken up in the present investigation (Tables 4, 5 and 7).

4. The superiority of four layer lamination scheme (either symmetric $0^0/90^0/90^0/0^0$ or antisymmetric $0^0/90^0/0^0/90^0$) is observed for simply supported hypar shells subjected to sinusoidal loadings (Table 6).

5. The relevant discussion on the results (Table 8) of free vibration analysis reveals the superiority of the C-C-C-C with regard to rigidity, followed by S-S-S-S and corner supported boundary conditions for all three shell forms (hyperbolic paraboloid, hypar and conoid).

Such increased rigidities are largely due to increased shell actions when h/R=-1/300 for hyperbolic paraboloid, c/a=0.2 for hypar and h_l/H_h = 0.2 for conoid shells when the other respective parameters are constants.

6. Authors' results of free vibration of conoids show the superiority of the clamped conoids having comparatively lower range (Figures 11 and 12). Simply supported conoids, however, show an increasing frequency initially with steep slope upto h_l/H_h around 0.3 and then with much reduced slopes (Figures 9 and 10).

ACKNOWLEDGEMENTS

The authors are thankful to the AICTE, New Delhi, for providing financial assistance to carry out this research work under the National Doctoral Fellowship Scheme.

APPENDIX A

Assuming $H_i = (z_{k+1}^i - z_k^i)/i$, where i=1, 7. The elements of the submatrices of the rigidity matrix are written in the following terms:

$$D_m = \sum_{k=1}^{N_L} \begin{bmatrix} \bar{Q}_{11}H_1 & \bar{Q}_{12}H_1 & \bar{Q}_{16}H_1 & \bar{Q}_{11}H_3 & \bar{Q}_{12}H_3 & \bar{Q}_{16}H_3 \\ & \bar{Q}_{22}H_1 & \bar{Q}_{26}H_1 & \bar{Q}_{12}H_3 & \bar{Q}_{22}H_3 & \bar{Q}_{26}H_3 \\ & & \bar{Q}_{66}H_1 & \bar{Q}_{16}H_3 & \bar{Q}_{26}H_3 & \bar{Q}_{66}H_3 \\ & & & \bar{Q}_{11}H_5 & \bar{Q}_{12}H_5 & \bar{Q}_{16}H_5 \\ & \text{Symm.} & & & \bar{Q}_{22}H_5 & \bar{Q}_{26}H_5 \\ & & & & & \bar{Q}_{66}H_5 \end{bmatrix}$$

The elements of D_c and D_b matrices can be obtained by replacing (H_1, H_3 and H_5) by (H_2, H_4 and H_6) and (H_3, H_5 and H_7) respectively, and

$$D_s = \sum_{k=1}^{N_L} \begin{bmatrix} \overline{Q}_{44}H_1 & \overline{Q}_{45}H_1 & \overline{Q}_{44}H_3 & \overline{Q}_{45}H_3 & \overline{Q}_{44}H_2 & \overline{Q}_{45}H_2 & \overline{Q}_{44}H_4 & \overline{Q}_{45}H_4 \\ & \overline{Q}_{55}H_1 & \overline{Q}_{45}H_3 & \overline{Q}_{55}H_3 & \overline{Q}_{45}H_2 & \overline{Q}_{55}H_2 & \overline{Q}_{45}H_4 & \overline{Q}_{55}H_4 \\ & & \overline{Q}_{44}H_5 & \overline{Q}_{45}H_5 & \overline{Q}_{44}H_4 & \overline{Q}_{45}H_4 & \overline{Q}_{44}H_6 & \overline{Q}_{45}H_6 \\ & & & \overline{Q}_{55}H_5 & \overline{Q}_{45}H_4 & \overline{Q}_{55}H_4 & \overline{Q}_{45}H_6 & \overline{Q}_{55}H_6 \\ & & & & \overline{Q}_{44}H_3 & \overline{Q}_{45}H_3 & \overline{Q}_{44}H_5 & \overline{Q}_{45}H_5 \\ & \text{Symm.} & & & & \overline{Q}_{55}H_3 & \overline{Q}_{45}H_5 & \overline{Q}_{55}H_5 \\ & & & & & & \overline{Q}_{44}H_7 & \overline{Q}_{45}H_7 \\ & & & & & & & \overline{Q}_{55}H_7 \end{bmatrix}$$

APPENDIX B

The inertia matrix [m] for the present higher-order theory is given by,

$$[m]=\begin{bmatrix} I_1 & 0 & 0 & 0 & I_2 & I_3 & 0 & 0 & I_4 \\ 0 & I_1 & 0 & -I_2 & 0 & 0 & I_3 & -I_4 & 0 \\ 0 & 0 & I_1 & 0 & 0 & 0 & 0 & 0 & 0 \\ 0 & -I_2 & 0 & I_3 & 0 & 0 & -I_4 & I_5 & 0 \\ I_2 & 0 & 0 & 0 & I_3 & I_4 & 0 & 0 & I_5 \\ I_3 & 0 & 0 & 0 & I_4 & I_5 & 0 & 0 & I_6 \\ 0 & I_3 & 0 & -I_4 & 0 & 0 & I_5 & -I_6 & 0 \\ 0 & -I_4 & 0 & I_5 & 0 & 0 & -I_6 & I_7 & 0 \\ I_4 & 0 & 0 & 0 & I_5 & I_6 & 0 & 0 & I_7 \end{bmatrix}$$

The parameters I_1, I_3 and (I_5, I_7) are linear inertia, rotary inertia and higher-order inertia terms, respectively. The parameters I_2, I_4 and I_6 are the coupling inertia terms and are expressed as follows:

$(I_1, I_2, I_3, I_4, I_5, I_6, I_7) = \sum_{k=1}^{N_L} \int_{z_k}^{z_{k+1}} (1, z, z^2, z^3, z^4, z^5, z^6)\rho_k dz$, where ρ_k is the material density of the k^{th} layer and the shape function matrix [N] is given by

$$[N]=\begin{bmatrix} N_i & & & & & & & & \\ & N_i & & & & & & & \\ & & N_i & & & & & & \\ & & & N_i & & & & & \\ & & & & N_i & & & & \\ & & & & & N_i & & & \\ & & & & & & N_i & & \\ & & & & & & & N_i & \\ & & & & & & & & N_i \end{bmatrix}$$

i=1,8 and N_i is the shape function for the node i.

REFERENCES

1. Reissner, E. (1945). The effect of transverse shear deformation on the bending of elastic plates. *ASME Journal of Applied mechanics*, 12(2): 69-77.
2. Mindlin, R.D. (1951). Influence of rotary inertia and shear in flexural motions of isotropic elastic plates. *ASME Journal of Applied mechanics*, 18(2): 31-38.
3. Yang, T.Y. (1973). High order rectangular shallow shell finite element. *Journal of the Engineering Mechanics Division*, 99(EM1): 157-181.
4. Reddy, J.N. and Liu, C.F. (1985). A higher-order shear deformation theory of laminated elastic shells. *Int. J. Engng. Sci.*, 23(3): 319-330.
5. Shu, X. and Sun, L. (1994). An improved simple higher-order theory for laminated composite plates. *Computers & Structures*, 50(2): 231-236.
6. Liew, K.M. and Lim, C.W. (1996). A higher-order theory for vibration of doubly curved shallow shells. *ASME, Journal of Applied Mechanics*, 63: 587-593.
7. Kant, T. and Khare, R.K. (1997). A higher-order facet quadrilateral composite shell element, *Int. J. for Numerical Methods in Engng.*, 40: 4477-4499.
8. Bhimaraddi, A. (1984). A higher order theory for free vibration analysis of circular cylindrical shells. *Int. J. Solids Structures*, 20(7): 623-630.
9. Mallikarjuna and Kant, T. (1992). A general fibre-reinforced composite shell element based on a refined shear deformation theory. *Computers & Structures*, 42(3): 381-388.
10. Cho, M., Kim, K. and Kim, M. (1996). Efficient higher-order shell theory for laminated composites. *Composite Structures*, 34(2): 197-212.
11. Choi, C.K. (1984). A conoidal shell analysis by modified isoparametric element, *Computers & Structures,* 18(5): 921-924.

12. Ghosh, B. and Bandyopadhyay, J.N. (1989). Bending analysis of conoidal shells using curved quadratic isoparametric element, *Computers & Structures,* 33(4): 717-728.

13. Ghosh, B. and Bandyopadhyay, J.N. (1990). Approximate bending analysis of conoidal shells using the Galerkin method, *Computers & Structures,* 36(5): 801-805.

14. Aditya, A.K. and Bandyopadhyay, J.N. (1989). Simplified bending analysis of doubly curved shells, *Computers & Structures,* 33(3): 781-784

15. Chakravorty, D., Bandyopadhyay, J.N. and Sinha, P.K. (1996). Finite element free vibration analysis of doubly curved laminated composite shells. *Journal of Sound and Vibration*, 191(4): 491-504.

16. Chakravorty, D., Bandyopadhyay, J.N. and Sinha, P.K. (1998). Application of FEM on free and forced vibration of laminated shells. *ASCE, Journal of Engineering Mechanics*, 124(1), 1-8.

17. Stavridis, L.T. (1998). Dynamic analysis of shallow shells of rectangular base. *Journal of Sound and Vibration*, 218(5): 861-882.

18. Nayak, A.N. and Bandyopadhyay, J.N. (2002). Free vibration analysis and design aids of stiffened conoid shells. *ASCE, J. Eng. Mech.,* 124(4): 419-427.

19. Nayak, A.N. and Bandyopadhyay, J.N. (2003). Free vibration analysis of laminated stiffened shells. *ASCE, J. Eng. Mech.,* 131(1): 100-105.

20. Moita, J.S., Soares, C.M.M. and Soares, C.A.M. (1999). Buckling and dynamic behavior of laminated composite structures using a discrete higher-order displacement model. *Computers &Structures*, 73(1-5): 407-423.

21. Khare, R.K., Kant, T. and Garg, A.K. (2004). Free vibration of composite and sandwich laminates with a higher-order facet shell element. *Composite Structures*, 65: 405-418.

22. Bhimaraddi, A. (1993). Three-dimensional elasticity solution for static response of orthotropic doubly curved shallow shells on rectangular planform, *Composite Structures*, 24(1): 67-77.

23. Pagano, N.J. (1970). Exact solutions for rectangular bidirectional composite and sandwich plates. *J. Comp. Materials,* 4: 20-34.

24. Reddy, J.N. (1984). A simple higher-order theory for laminated composite plates. *ASME, Journal of Applied Mechanics*, 51: 745-752.

Full Address of Authors

1. Pradyumna S. (Corresponding author)
National Doctoral Fellow,
Department of Civil Engineering,
Indian Institute of Technology Kharagpur,
Kharagpur, West Bengal,
India 721 302
E-mail: pradyumna@civil.iitkgp.ernet.in

2. Prof. J.N. Bandyopadhyay,
Department of Civil Engineering,
Indian Institute of Technology Kharagpur,
Kharagpur, West Bengal,
India 721 302
Phone: +91-3222-283404
Fax: +91-3222-282254
E-mail: jnb@civil.iitkgp.ernet.in

Figure captions

Figure 1. Conoid (CON)

Figure 2. Hyparbolic paraboloid (HPR)

Figure 3. Hypar (HYP)

Figure 4. Laminated composite doubly curved shell element

Figure 5. Lamina reference axis and fibre orientation

Figure 6. Convergence of displacement values

Figure 7. Variation of transverse displacement (w) along $\bar{x} = 0.5$

Figure 8. Variation of transverse displacement (w) along $\bar{y} = 0$

Figure 9. Effect of h_l / H_h ratio on the non-dimensional frequencies of a S-S-S-S conoid shell with $a / H_h = 2.5$

Figure 10. Effect of h_l / H_h ratio on the non-dimensional frequencies of a S-S-S-S conoid shell with $a / H_h = 5$

Figure 11. Effect of h_l / H_h ratio on the non-dimensional frequencies of a C-C-C-C conoid shell with $a / H_h = 2.5$

Figure 12. Effect of h_l / H_h ratio on the non-dimensional frequencies of a C-C-C-C conoid shell with $a / H_h = 5$

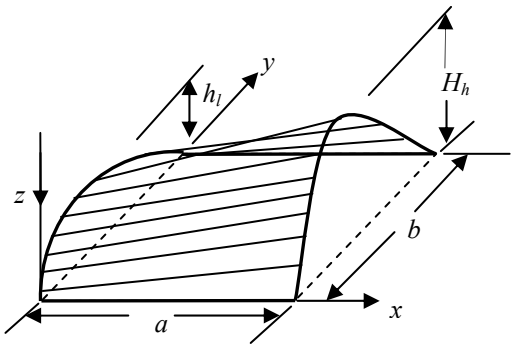

$$z = 4\{h_l + (H_h - h_l)\frac{x}{a}\}\left(\frac{y^2}{b^2} - \frac{y}{b}\right)$$

Figure 1.

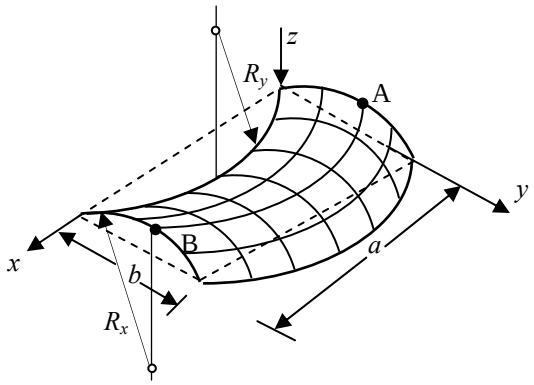

Figure 2.

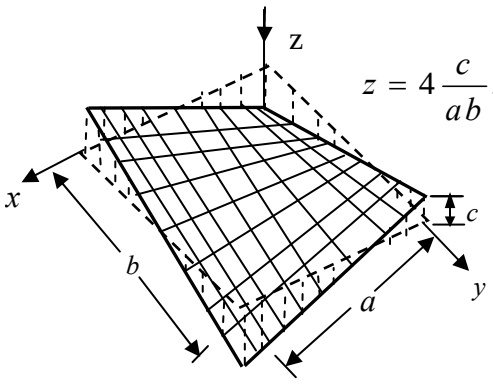

$$z = 4\frac{c}{ab}xy + cx/a + cy/b$$

Figure 3.

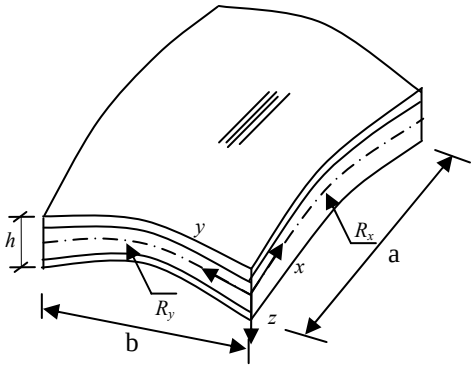

Figure 4.

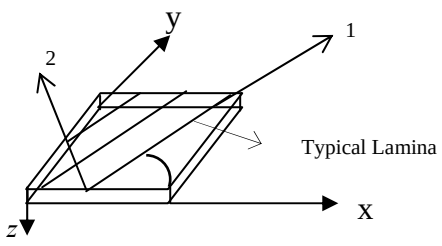

Figure 5.

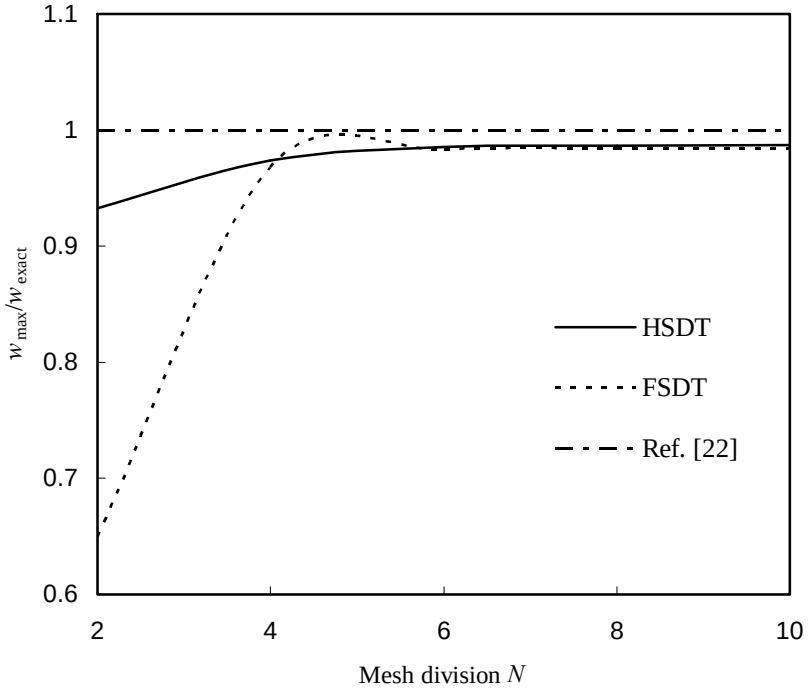

Figure 6.

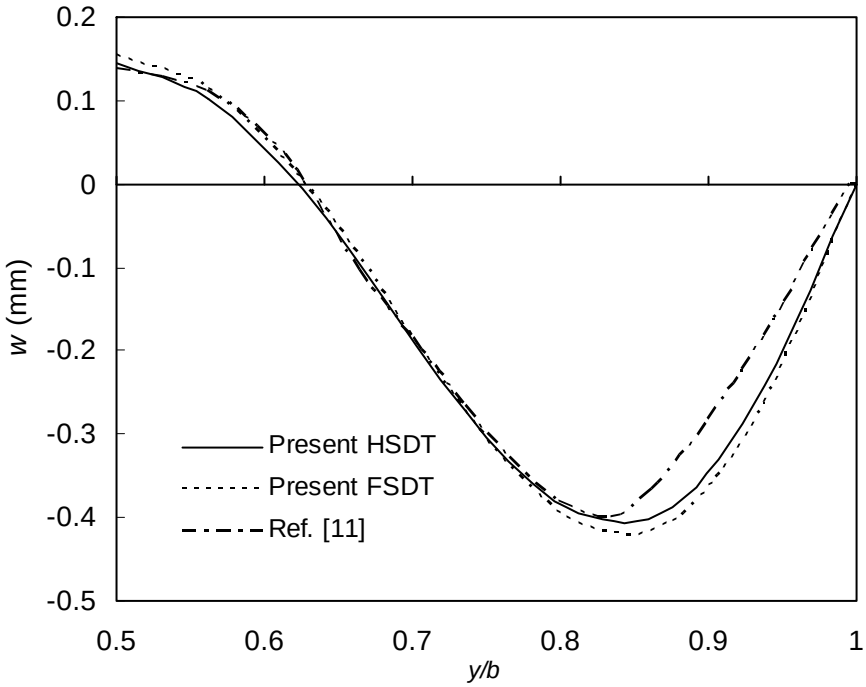

Figure 7.

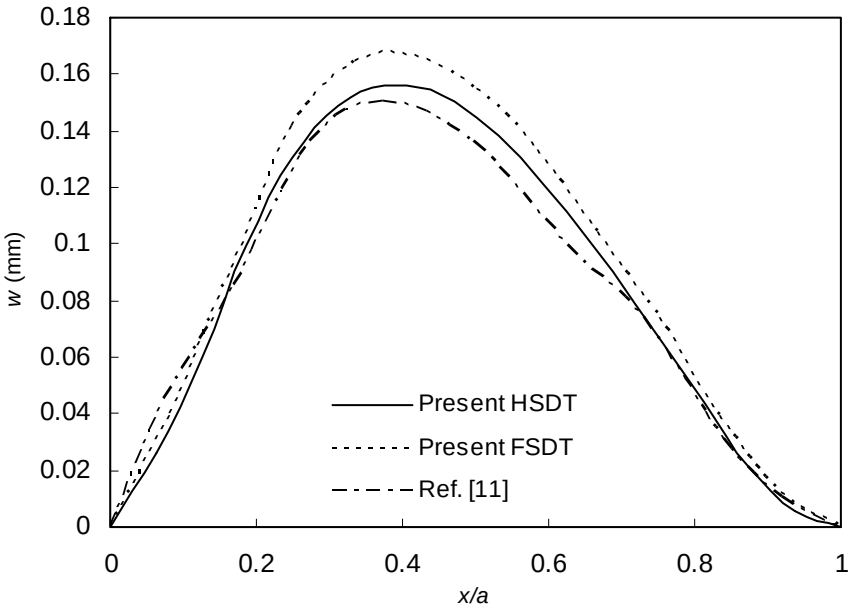

Figure 8.

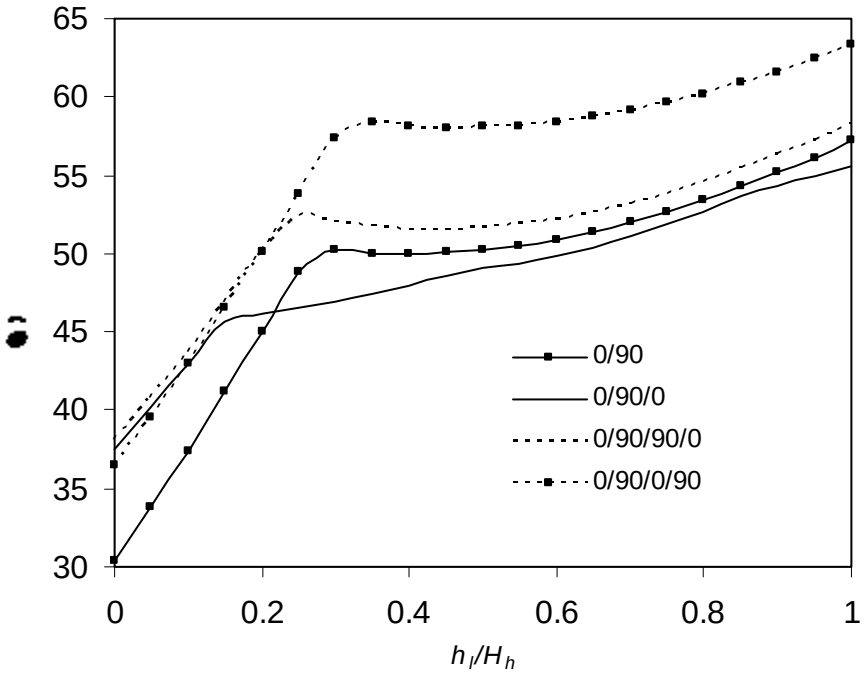

Figure 9.

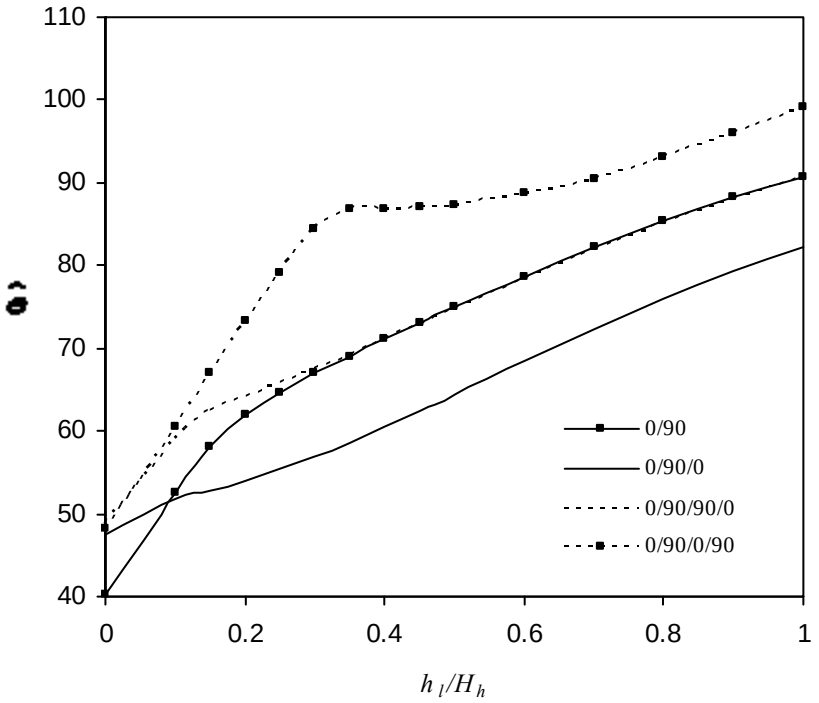

Figure 10.

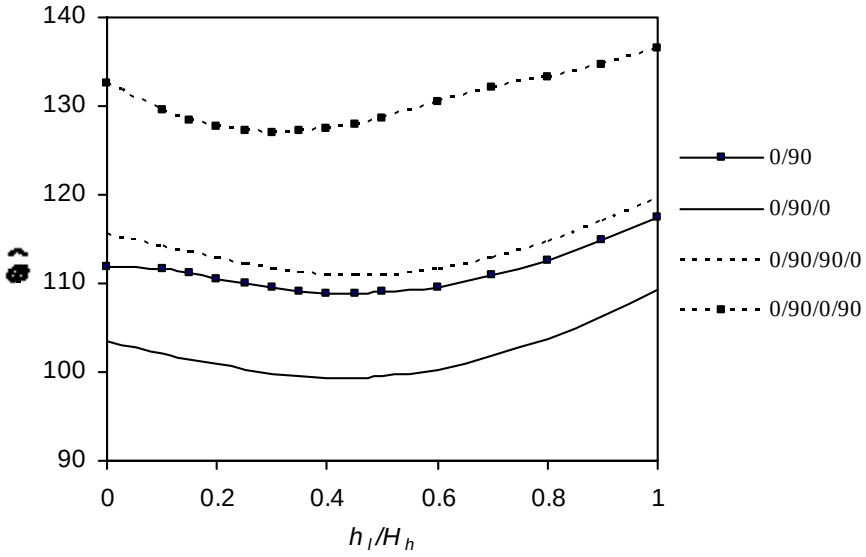

Figure 11.

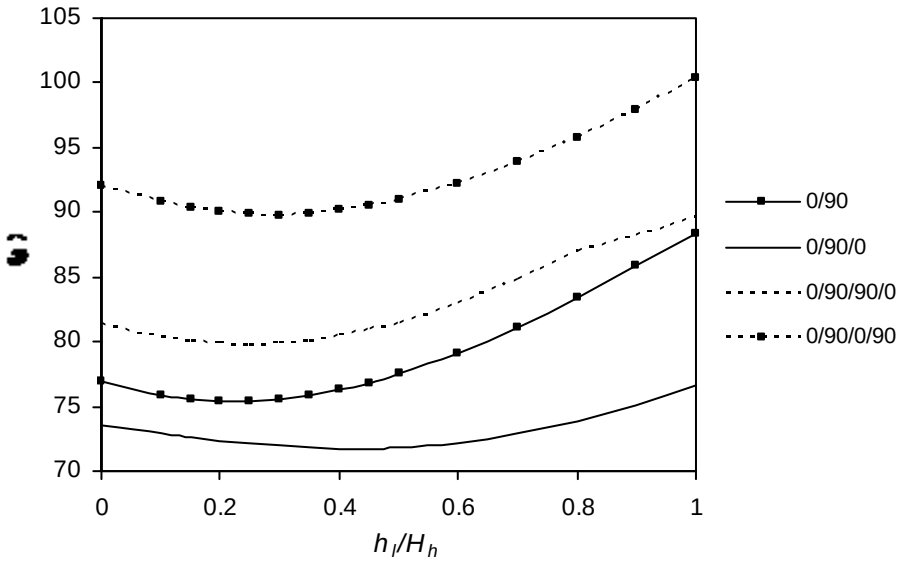
105
100
95
90
85
80
75
70
0
0.2
0.4
0.6
0.8
1
h_l/H_h
0/90
0/90/0
0/90/90/0
0/90/0/90

Figure 12.

Table captions

Table 1 Non-dimensional center deflection of cross-ply laminated plate (b/a=3)

Table 2 Non-dimensional centre displacements of SS1 spherical shell subjected to sinusoidal loading.

Table 3 Non-dimensional frequencies $\bar{\omega}$ of simply supported cross-ply $[0^0/90^0]_4$ laminated composite shells

Table 4 Non-dimensional central deflection $\bar{w}$ for simply supported cross-ply laminated hypar shells subjected to uniformly distributed load

Table 5 Non-dimensional central deflection $\bar{w}$ for cross-ply laminated clamped hypar shells subjected to uniformly distributed load

Table 6 Non-dimensional central deflection $\bar{w}$ for cross-ply laminated simply supported hypar shells subjected to sinusoidal load

Table 7 Non-dimensional central deflection $\bar{w}$ for cross-ply laminated clamped hypar shells subjected to sinusoidal load

Table 8 Non-dimensional frequency parameter $\bar{\omega}$ for different types of antisymmetric angle ply $\theta^0/-\theta^0$ laminate shells.

Table 1

a/h	Present FSDT	Present HSDT	Reddy [24]	Pagano [23]
4	2.3567	2.6436	2.6411	2.82
10	0.8021	0.8683	0.8622	0.919
20	0.5782	0.5956	0.5937	0.610
100	0.5064	0.5071	0.507	0.508

Table 2

		Single layer orthotropic			0/90		
R/a		*h/a*=0.01	*h/a*=0.1	*h/a*=0.15	*h/a*=0.01	*h/a*=0.1	*h/a*=0.15
1	Bhimaraddi [22]	75.397	4.7117	2.5641	54.129	4.6920	2.7386
	FSDT	74.1985	3.4573	1.7293	53.4962	3.7840	1.9856
	HSDT	74.3969	3.8226	1.9481	53.5448	4.0216	2.1687
2	Bhimaraddi [22]	285.72	5.9693	2.6788	212.33	8.8092	3.8190
	FSDT	282.3650	5.2680	2.3306	210.8660	7.8942	3.3338
	HSDT	283.0607	5.4683	2.4157	211.0061	8.1085	3.4146
3	Bhimaraddi [22]	593.43	6.2215	2.6635	456.46	10.512	4.0856
	FSDT	587.5019	5.8336	2.4909	463.0167	9.8813	3.8131
	HSDT	588.8315	5.9359	2.5253	463.2959	9.9778	3.8168
4	Bhimaraddi [22]	953.25	6.3014	2.6494	799.81	11.263	4.1758
	FSDT	944.8427	6.0614	2.5524	796.2405	10.8358	4.0152
	HSDT	946.7702	6.1186	2.5659	796.6894	10.8526	3.9805
5	Bhimaraddi [22]	1325.5	6.3332	2.6393	1198.7	11.639	4.2131
	FSDT	1315.0579	6.1729	2.5818	1193.9434	11.3430	4.1161
	HSDT	1317.4404	6.2069	2.5851	1194.5739	11.3115	4.0611
10	Bhimaraddi [22]	2767.7	6.3593	2.6256	3584 8	12.150	4.2457
	FSDT	2753.6250	6.3282	2.6222	3574.1976	12.0980	4.2589
	HSDT	2756.1901	6.3286	2.6111	3575.4383	11.9871	4.1737
∞	Bhimaraddi [22]	4343.0	6.3343	2.5879	10674.0	12.257	4.1291
	FSDT	4333.9229	6.3817	2.6360	10654.1719	12.3725	4.3087
	HSDT	4333.7875	6.3702	2.6199	10652.4018	12.2305	4.2126

Table 3

Shell Type	Ref. [19]	Present FSDT	Present HSDT
Elliptic paraboloid	47.384	47.380	47.341
Hyperbolic paraboloid	14.743	14.742	14.596
Hypar	52.002	52.014	51.291
Conoid	81.097	80.981	80.918

Note: a/b=1, a/h=100, for elliptic paraboloid, h/R_x= h/R_y =1/300; for hyperbolic paraboloid, h/R_x= -h/R_y =1/300; for hypar, c/a=0.2; for conoid, a/H_h=2.5, h_l/H_h = 0.25;

Table 4

c/a	$(0^0/90^0)$	$(0^0/90^0/0^0)$	$(0^0/90^0/90^0/0^0)$	$(0^0/90^0/0^0/90^0)$
0	16.9763	**6.7055**	6.8436	8.1137
0.05	2.3774	**1.8988**	1.9629	2.0922
0.10	0.6193	**0.5680**	0.5972	0.6252
0.15	0.2610	**0.2493**	0.2638	0.2767
0.20	0.1388	**0.1360**	0.1434	0.1504

Note: $a/b=1; a/h=100; E_1/E_2=25; G_{23}=0.2E_2; G_{12}=G_{13}=0.5E_2; \nu_{12}=0.25$

Table 5

c/a	$(0^0/90^0)$	$(0^0/90^0/0^0)$	$(0^0/90^0/90^0/0^0)$	$(0^0/90^0/0^0/90^0)$
0	3.9672	**1.4189**	1.4859	1.7894
0.05	1.3371	**0.8008**	0.8459	0.9640
0.10	0.3901	**0.3265**	0.3451	0.3791
0.15	0.1576	**0.1564**	0.1613	0.1732
0.20	**0.0805**	0.0880	0.0879	0.0917

Note: $a/b=1; a/h=100; E_1/E_2=25; G_{23}=0.2E_2; G_{12}=G_{13}=0.5E_2; \nu_{12}=0.25$

Table 6

c/a	$(0^0/90^0)$	$(0^0/90^0/0^0)$	$(0^0/90^0/90^0/0^0)$	$(0^0/90^0/0^0/90^0)$
0	10.6524	**4.3430**	4.3441	5.0857
0.05	1.6785	1.3973	**1.3511**	1.3866
0.10	0.5672	0.5390	0.4966	**0.4781**
0.15	0.3167	0.2966	0.2716	**0.2545**
0.20	0.2180	0.1974	0.1800	**0.1680**

Note: $a/b=1; a/h=100; E_1/E_2=25; G_{23}=0.2E_2; G_{12}=G_{13}=0.5E_2; \nu_{12}=0.25$

Table 7

c/a	$(0^0/90^0)$	$(0^0/90^0/0^0)$	$(0^0/90^0/90^0/0^0)$	$(0^0/90^0/0^0/90^0)$
0	2.8703	**1.0783**	1.0967	1.2944
0.05	1.0168	**0.6331**	0.6440	0.7138
0.10	0.3335	**0.2783**	0.2826	0.2988
0.15	0.1524	**0.1420**	0.1433	0.1484
0.20	0.0852	**0.0836**	0.0837	**0.0836**

Note: $a/b=1; a/h=100; E_1/E_2=25; G_{23}=0.2E_2; G_{12}=G_{13}=0.5E_2; \nu_{12}=0.25$

Table 8

θ^0	Hyperbolic paraboloid shell h/R_y (R_x=-R_y)				
C-C-C-C	-1/300	-1/500	-1/750	-1/1000	0
15	71.9689	64.8192	54.5169	44.2070	24.1361
30	64.5320	51.6167	38.0747	31.7184	20.5975
45	49.7410	33.8265	26.9788	24.1255	19.8621
S-S-S-S (SS2)					
15	54.9783	46.3938	43.3198	41.4780	12.6750
30	52.0557	41.0520	35.1199	27.7013	12.0742
45	47.1527	30.0847	22.0836	18.4693	12.3423
Corner supported					
15	8.7098	6.9390	5.6789	5.0255	3.8113
30	8.5902	7.0953	6.0674	5.5420	4.5297
45	8.4482	7.1207	6.3417	5.9861	5.4336
Hypar shell (*c/a*)					
C-C-C-C	0.20	0.15	0.1	0.05	0
15	121.1150	102.7400	84.4587	53.2526	24.1361
30	116.0076	104.0245	91.1993	63.6122	20.5975
45	118.9551	101.4451	85.6254	69.5167	19.8621
S-S-S-S (SS2)					
15	93.4221	78.0224	63.0787	40.4870	12.6750
30	92.6757	77.4935	59.1837	42.8307	12.0742
45	95.5267	80.3689	67.0237	43.4276	12.3423
Corner supported					
15	12.0714	12.1429	12.0506	11.4118	3.8113
30	12.1957	12.0471	11.8974	11.6903	4.5297
45	10.6905	10.3020	9.9852	9.7759	5.4336
Conoid shell (h_l/H_h) , a/H_h=5					
C-C-C-C	0.20	0.15	0.10	0.05	0
15	65.6122	63.7285	61.8627	60.0667	58.3857
30	71.3619	68.1776	65.3564	62.5348	60.1323
45	81.3614	77.6831	74.0710	70.6078	67.3693
S-S-S-S (SS2)					
15	52.7427	52.3790	51.0267	49.5872	48.1619
30	59.0493	57.0236	54.8623	52.7309	50.7304
45	68.1662	65.3149	62.3482	59.4125	56.6474
Corner supported					
15	16.9478	15.3246	13.2651	11.1673	9.6770
30	18.6549	16.7780	14.4917	12.2324	10.6670
45	21.0430	19.3262	16.8132	13.9950	11.9568